

# Josephson effect and tunneling spectroscopy in Nb/Al<sub>2</sub>O<sub>3</sub>/Al/MgB<sub>2</sub> thin films junctions

G. Carapella<sup>1</sup>, N. Martucciello<sup>1</sup>, G. Costabile<sup>1</sup>, C. Ferdeghini<sup>2</sup>, V. Ferrando<sup>2</sup>, and G. Grassano<sup>2</sup>

<sup>1</sup>*INFN Research Unit and Department of Physics "E. R. Caianiello", University of Salerno, I-84081 Baronissi, Italy.*

<sup>2</sup>*INFN Research Unit and Department of Physics, University of Genova, I-16146 Genova, Italy.*

(October 24, 2018)

We report the demonstration of dc and ac Josephson effects as well as tunneling spectroscopy measurements on Nb/Al<sub>2</sub>O<sub>3</sub>/Al/MgB<sub>2</sub> thin films heterostructures. Data on dc Josephson effect suggest the presence of two characteristic critical currents possibly accounted for the presence of two gaps in the MgB<sub>2</sub> film. Tunneling spectroscopy measurements confirm the two-gap scenario and are explained with the presence of tunneling both from dirty limit regions, reflecting an order parameter  $\Delta_{dirty} \approx 2$  meV, and from clean limit regions, reflecting an order parameter  $\Delta_{3D} \approx 0.9$  meV. The temperature dependence, the magnitudes and the relevant ratios of these two gaps are found in good agreement with the predictions of a recently proposed multigap theory. The value of the larger gap component estimated from conductance spectra is found to be consistent with the one deduced from Josephson coupling.

74.50.+r,74.80.Fp,85.25.Dq

The recent demonstration of superconductivity [1] at 39 K in MgB<sub>2</sub> has attracted considerable interest with regard to both fundamental issues and practical applications. Though several quasiparticle tunneling experiments [2–11] with normal contacts have been performed to measure the energy gap, only few experiments [12–15] to probe the Josephson effects in this new material have been performed. To date, only nanobridges [14] and localized ion damage Josephson junctions [15] have been successfully tested on MgB<sub>2</sub> films. To fully exploit the possibility of superconducting electronic to cryocooler temperature promised by this new material, a further effort toward realization and study of Josephson junctions based on MgB<sub>2</sub> films is again necessary.

In this letter, we report Josephson effect and tunneling spectroscopy analysis on Nb/Al<sub>2</sub>O<sub>3</sub>/Al/MgB<sub>2</sub> thin films junctions. At our knowledge, this is the first demonstration of Josephson effects in a MgB<sub>2</sub> film based heterostructure. Experimental data on dc Josephson effect indicate the presence of two classes of hysteretic Josephson junctions with two characteristic critical currents accounting for probable presence of two gaps in the MgB<sub>2</sub> film. Experimental data on tunneling spectroscopy measurements confirm this two-gap scenario and are accounted for the presence of tunneling both from dirty limit regions, reflecting an order parameter  $\Delta_{dirty}$ , and from clean limit regions, reflecting an order parameter  $\Delta_{3D}$ . The temperature dependence deduced from tunneling spectroscopy gives for the dirty limit region  $\Delta_{dirty}(0) \approx 2$  meV,  $T_c^{dirty} = 14.5$  K and for the clean limit region  $\Delta_{3D}(0) \approx 0.9$  meV,  $T_c \approx 29.5$  K, with measured ratios  $2\Delta_{dirty}(0)/k_B T_c^{dirty} = 3.5$ ,  $\Delta_{dirty}/\Delta_{3D} \approx 2.2$  in good agreement with the predictions of the recently proposed multigap theory [16] of Liu *et al.*

*The junctions-* The MgB<sub>2</sub> films were deposited at room temperature on Al<sub>2</sub>O<sub>3</sub> substrate by Pulsed Laser Depo-

sition (PLD), starting from stoichiometric target. We used sintered target prepared by direct synthesis from the elements. The PLD experimental apparatus consists of an UHV deposition chamber and a KrF excimer laser; details of the apparatus are described elsewhere [17]. The as-deposited amorphous films, about 500 nm thick, were ex-situ annealed in magnesium vapor. The samples were placed in a sealed tantalum tube, in Ar atmosphere, containing Mg lumps (approximately 0.05 mg/cm<sup>3</sup>), and then they were placed in an evacuated quartz tube and heated at  $T = 1120$  K for 30 minutes followed by rapid quenching at room temperature. The MgB<sub>2</sub> films resulted to be strongly c-axis oriented as determined using synchrotron radiation at the ID32 beamline of ESRF. The films show a surface RMS roughness of about 15 nm as proved by AFM measurements, a critical temperature ranging from 33 K to 37 K and a maximum residual resistivity ratio of 2.5. Further details on the electrical, structural and morphological film characterization are reported in Ref. [18].

To realize the junctions, we avoided wet photolithographic techniques, that could damage the surface of the MgB<sub>2</sub>. For the bottom electrode (MgB<sub>2</sub>) definition, we developed a special setup inside the growth chamber for the in-situ use of tantalum shadow masks. Therefore the precursor was directly deposited in shape of narrow strip (about 200  $\mu$ m wide) and then annealed in Mg atmosphere. Before the definition of the superconducting counter-electrode (Nb), the MgB<sub>2</sub> film was sputter-etched for about 10 nm in Ar atmosphere, to reduce the thickness of the weakened surface layer growth after exposition to air. An Al/Al<sub>2</sub>O<sub>3</sub>/Nb structure was then fabricated in-situ on the whole substrate. The 10 nm thick Al and the 500 nm thick Nb films were rf sputtered while the  $\sim 2$  nm thick Al<sub>2</sub>O<sub>3</sub> was thermally growth in pure oxygen atmosphere. The Al/Al<sub>2</sub>O<sub>3</sub>/Nb structure was finally patterned by Reactive Ion Etching with the

geometry of the counter-electrode, a 40  $\mu\text{m}$  wide strip. The cross geometry [see inset of Fig. 1(a)] of the fabricated junctions allows us to make four contacts measurements. We fabricated and tested three of these junctions with similar results. The heterostructures showed a good thermal cyclability. For the junction we report here the critical temperature of the Nb counter-electrode was  $T_c^{\text{Nb}}=7.2$  K and the critical temperature of the  $\text{MgB}_2$  electrode was  $T_c^{\text{MgB}_2}=33$  K.

*Josephson effect-* Figure 1(a) shows the current-voltage (IV) curve of the junction recorded at  $T=4.2$  K. The current branch a  $V = 0$  clearly suggests the evidence for a dc Josephson effect in the junction. However, the resistive characteristic appears quite complex. Two distinct resistive families can be observed, starting with two slightly different critical Josephson currents. Within the same resistive family, slightly different resistive branches are exhibited, meaning that we are in fact concerned with a disordered array of smaller Josephson junctions with comparable critical currents. Moreover, also the magnetic field diffraction pattern we observed is typical of a disordered array of small area Josephson junctions: very irregular, with fast field modulation over a quite large current background.

Curves in Fig. 1(a) are recorded with a 100 Hz current sweep, so that a superposition of both families is plotted. In dc biasing, it is possible to record one of the two resistive families, mainly the curve corresponding to the larger Josephson critical current, as shown in the inset of Fig. 1(a). The evolution in temperature of such hysteretic IV curve is shown in Fig. 1(b). The quite large thermal smearing envisaged in the IV curves at 4.2 K is compatible with the idea that our junction consists of a parallel arrays of about 200 small junctions with individual critical currents of about 10  $\mu\text{A}$ . The total critical current as a function of the temperature is plotted in Fig. 1(c). The behavior is qualitatively similar to the one exhibited [19] in proximity coupled  $S_1INS_2$  structures, with a  $N$  layer thicker than the 10 nm Al layer we deposited. This means that the normal surface layer on the  $\text{MgB}_2$  was not completely removed with our sputter etch cleaning procedure.

Figure 1(a) seems indicate the presence of two qualitatively different Josephson junctions classes, possibly corresponding to two energy gaps in the  $\text{MgB}_2$  film. In this framework, an estimate of the larger gap can be made from IV curve shown in the inset of Fig. 1(a), corresponding to the larger of the two possible critical currents we can envisage in the main panel. Here, by assuming comparable values for the critical currents of the junctions in the array, we can estimate a mean characteristic voltage  $V_c \equiv I_c R_N \approx 2.3$  mV. With a critical temperature of 7.2 K, a gap  $\Delta_1 \simeq 1.1$  meV is found for our Nb. The gap component  $\Delta_2$  of  $\text{MgB}_2$  responsible of the higher critical current Josephson junction class can then estimated from relation [19]

$$I_c R_N \simeq \frac{\pi}{e} \frac{\Delta_1 \Delta_2}{\Delta_1 + \Delta_2} \quad (1)$$

as  $\Delta_2 = (2.1 \pm 0.1)$  meV at 4.2 K.

The Josephson nature of the  $V = 0$  branch exhibited in our IV curve is confirmed by the regular appearance of Shapiro steps (ac Josephson effect) when the junctions is irradiated with rf signals in the microwave range. The steps are expected at voltages  $V_n = n\Phi_0\nu$ , where  $n$  is an integer,  $\Phi_0$  is the flux quantum, and  $\nu$  is the frequency of the applied radiation. Figure 2 shows these steps induced in the IV curve of the junction irradiated with microwaves signals of different power levels. As expected, the voltage spacing of the steps is found to be 20.7  $\mu\text{V}$  for microwave power at frequency  $\nu = 10.01$  GHz [Fig. 2(a)], and 27.8  $\mu\text{V}$  at frequency  $\nu = 13.45$  GHz [Fig. 2(b)].

*Tunneling spectroscopy-* Figure 3(a) shows the IV curves recorded at temperatures near the transition temperature of the Nb electrode. The curves are now quite smooth, as better seen from differential conductances  $dI/dV$  shown in Fig. 3(b). These conductance curves were obtained by numerically differentiating the curves in Fig. 3(a). When the Josephson peak at  $V = 0$  completely disappears, we are concerned with a  $N_1IS_2$  junction ( $N_1 = \text{Nb}$  in the normal state,  $S_2 = \text{MgB}_2$  in the superconducting state) and a tunneling spectroscopy of the proximized surface layer of the  $\text{MgB}_2$  is possible.

The differential conductance  $G(V) \equiv dI/dV(V)$  can be fitted using the functional form for a  $NIS$  contact

$$G \sim \frac{d}{dV} \int_{-\infty}^{\infty} \rho(E + eV) [f(E) - f(E + eV)] dE, \quad (2)$$

where  $\rho(E) = \text{Re} \left\{ (E - i\Gamma) / [(E - i\Gamma)^2 - \Delta^2]^{1/2} \right\}$  is the modified [20] BCS density of states,  $\Delta(T)$  is the fitted energy gap,  $\Gamma(T)$  is the fitted gap-smearing parameter, and  $f(E)$  is the Fermi function. The best one-gap fit of the conductance curve of our junction a  $T=7.7$  K is shown in Fig. 3(c). For this temperature  $\Delta = (2.2 \pm 0.2)$  meV,  $\Gamma = 0.9$  meV are estimated for the  $\text{MgB}_2$  film.

Figure 4(a) shows the normalized differential conductances curves for temperature increasing up the critical temperature of the  $\text{MgB}_2$  electrode. The small parabolic background envisaged in the curves suggests a moderate barrier height for the contact, probably below 100 meV. Moreover, the quite large zero bias conductance means the presence of appreciable leakage currents. The gap structure completely disappears at  $T=29.5$  K, lower than the critical temperature of 33 K measured for the bulk electrode, meaning that we are probing proximized surface layer of the  $\text{MgB}_2$  with weakened superconductivity.

From the fit of the conductance curves in Fig. 4(a) with one-gap model Eq. (2) the temperature dependence of the energy gap shown in Fig. 4(b) is obtained. The curves are reasonably well fitted using a gap-smearing parameter  $\Gamma(T) \simeq 0.4\Delta(T)$ . The obtained temperature dependence of the energy gap clearly deviates from single gap BCS

behavior. Rather, data in Fig. 4(a) suggest the superposition of two BCS-like gaps with two different critical temperatures, a behavior very similar to the one recently observed [6] in tunneling spectroscopy on MgB<sub>2</sub> wires. Indeed, many recent experimental results from tunneling measurements [6,7,9,10], high resolution photoemission spectroscopy [21], microwave surface resistance [22], and heat specific measurements [23], are explained within a two-gap scenario in MgB<sub>2</sub>. On the other hand, many other tunneling and point-contact spectroscopy measurements [2–5,8,11,13] are explained assuming a single BCS-like gap in MgB<sub>2</sub>.

The multigap model proposed by Liu *et al.* [16] could explain this complex experimental scenario. In the clean limit [16], two different order parameters exist, a gap  $\Delta_{2D}$  accounting for current transport along B planes (a-b planes), and a gap  $\Delta_{3D}$  accounting for current transport in direction perpendicular to the B layers (c-axis). The gap  $\Delta_{3D}$  is three times smaller than the gap  $\Delta_{2D}$  and both gaps close to the critical temperature  $T_c$  of the MgB<sub>2</sub>, following a BCS-like temperature dependence. Moreover, the  $2\Delta_{2D}(0)/k_B T_c$  ratio is expected larger than the BCS value, while the  $2\Delta_{3D}(0)/k_B T_c$  ratio is expected lower than this value. In the dirty limit [16], the enhanced defect scattering leads to an averaging of both order parameters that results to an isotropic order parameter  $\Delta_{dirty}$  closing to a critical temperature  $T_c^{dirty}$  lower than the clean limit  $T_c$ . The magnitude  $\Delta_{dirty}$  is between the magnitudes of  $\Delta_{2D}$  and  $\Delta_{3D}$ , and the  $2\Delta_{dirty}(0)/k_B T_c^{dirty}$  ratio is the BCS value.

As stated above, our MgB<sub>2</sub> films resulted to be strongly c-axis oriented, and from geometry of our junction a tunneling along c-axis is expected, with spectra reflecting symmetry of  $\Delta_{3D}$  order parameter. On the other hand, due to the quite large area ( $200 \times 40$ )  $\mu\text{m}^2$  we are probing, we cannot exclude the presence of dirty regions in the contact area. The presence of these dirty regions is compatible with the quite large values of smearing parameter  $\Gamma$  we have found. Thus our junction can be considered as the parallel connection of two junctions corresponding to the tunneling into the dirty and clean regions, respectively. Thus, our measured conductance can be described by

$$G(V) = \alpha G(V, \Delta_{3D}) + (1 - \alpha)G(V, \Delta_{dirty}), \quad (3)$$

where  $0 < \alpha < 1$ , and the functional form  $G(V)$  is again Eq. (2). The temperature dependence of the two gaps deduced from the fit of the data in Fig. 4(a) with the two-gap model Eq. (3) is shown in Fig. 4(c). The best fit was obtained with  $\alpha = 0.5$ , meaning that clean limit and dirty limit regions was present in equal proportions in our tunnel contact. The fit with BCS functional temperature dependence gives for the clean limit  $\Delta_{3D}(0) = (0.9 \pm 0.1)$  meV,  $T_c \approx 29.5$  K and for the dirty limit  $\Delta_{dirty}(0) = (2.0 \pm 0.2)$  meV,  $T_c^{dirty} \approx 14.5$  K, with measured ratios  $2\Delta_{dirty}(0)/k_B T_c^{dirty} \simeq 3.5$ ,  $\Delta_{dirty}/\Delta_{3D} \approx 2.2$  in good agreement with the predictions of Liu *et al.*

The two gaps we have invoked for the explanation of two Josephson critical currents can be now identified with  $\Delta_{dirty}$  and  $\Delta_{3D}$ , with  $\Delta_{dirty}$  accounting for the larger Josephson critical current. In fact, from  $I_c R_N$  product we have estimated the larger gap component amplitude  $\Delta_2 = (2.1 \pm 0.1)$  meV, that is consistent with the  $\Delta_{dirty}(0) = (2.0 \pm 0.2)$  meV we have found from tunneling spectra analysis.

Summarizing, we have demonstrated dc and ac Josephson effect and we have analyzed tunneling spectroscopy measurements in a rather large area Nb/Al<sub>2</sub>O<sub>3</sub>/Al/MgB<sub>2</sub> thin films junction we have fabricated. The analysis of the dc IV curves has indicated the presence two characteristic Josephson critical currents, probably accounted for the presence of two gaps in the MgB<sub>2</sub> film. The tunneling spectroscopy measurements have confirmed this two-gap scenario and have been explained in the framework of the multigap theory of Liu *et al* with the presence of tunneling both from dirty limit regions, reflecting an order parameter  $\Delta_{dirty} \approx 2$  meV, and from clean limit regions, reflecting an order parameter  $\Delta_{3D} \approx 0.9$  meV. Experimental data have been found in good quantitative agreement with the predictions of Liu *et al.*

We acknowledge Dr. F. Giubileo and Dr. F. Bobba for useful discussions on tunneling spectra analysis. Financial support of MURST COFIN00 is also acknowledged.

- 
- [1] J. Nagamatsu *et al.*, Nature **410**, 63 (2001).
  - [2] G. Karapetrov *et al.*, Phys. Rev. Lett. **86**, 4374 (2001).
  - [3] S. Schmidt *et al.*, Phys. Rev. B **63**, 220504 (2001).
  - [4] G. Rubio-Bollinger *et al.*, Phys. Rev. Lett. **86**, 5582 (2001).
  - [5] K. Kohen *et al.*, cond-mat/0103512 (2001).
  - [6] A. Plecenik *et al.*, cond-mat/0104038 (2001).
  - [7] P. Szabo *et al.*, cond-mat/0105598 (2001).
  - [8] A. Sharoni *et al.*, Phys. Rev. B **63**, 22058 (2001).
  - [9] F. Giubileo *et al.*, cond-mat/0105146 (2001).
  - [10] F. Giubileo *et al.*, cond-mat/0105592 (2001).
  - [11] R. S. Gonnelli *et al.*, cond-mat/0107239 (2001).
  - [12] R. S. Gonnelli *et al.*, cond-mat/0103241 (2001).
  - [13] Y. Zhang *et al.*, cond-mat/0107478 (2001).
  - [14] A. Brinkman *et al.*, cond-mat/0103535 (2001).
  - [15] G. Burnell *et al.*, cond-mat/0106562 (2001).
  - [16] A. Liu *et al.*, cond-mat/0103570 (2001).
  - [17] M. R. Cimberle *et al.*, IEEE Trans. on Appl. Sup. **9**, 1727 (1999).
  - [18] C. Ferdeghini *et al.*, cond-mat/0107031 (2001).
  - [19] A. Barone and G. Paternó, *Physics and Applications of the Josephson Effect* (John Wiley & Sons, New York, 1982).
  - [20] R. C. Dynes *et al.*, Phys. Rev. Lett. **41**, 1509 (1978).
  - [21] S. Tsuda *et al.*, cond-mat/0104489 (2001).
  - [22] A. A. Zhukov *et al.*, cond-mat/0103587 (2001).
  - [23] Y. Wang *et al.*, cond-mat/0103181 (2001).

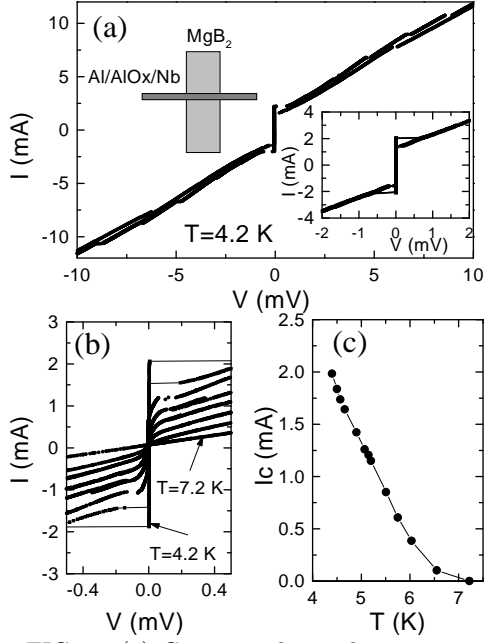


FIG. 1. (a) Current-voltage characteristic of the junction recorded at  $T = 4.2$  K showing resistive branches starting with different Josephson critical currents. In the insets, the IV curve with larger critical current and a sketch of the junction geometry are shown. (b) IV curves recorded at temperatures increasing from  $T = 4.2$  K to  $T = 7.2$  K. (c) Josephson critical current versus temperature.

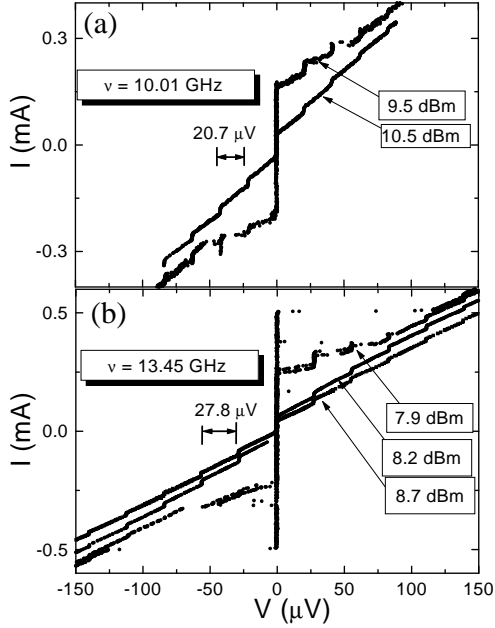


FIG. 2. IV curves of the junction showing Shapiro steps induced by a microwave signal with different power level. The frequency is  $\nu = 10.01$  GHz in (a) and  $\nu = 13.45$  GHz in (b). The curves are recorded at  $T = 4.2$  K.

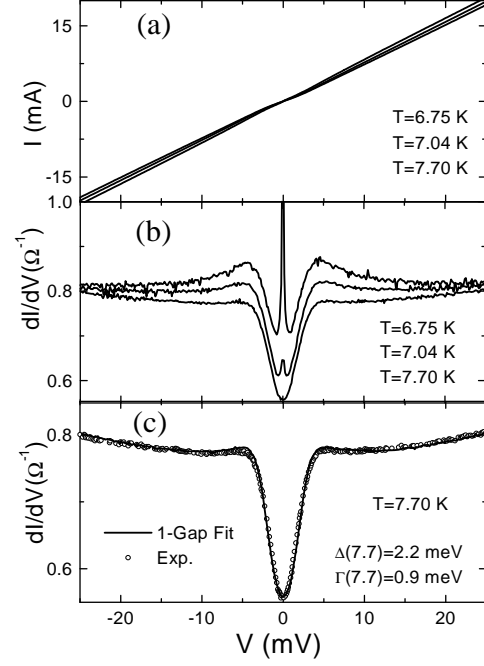


FIG. 3. IV curves (a) and differential conductances (b) at temperatures around the critical temperature of the Nb electrode. (c) Best fit (solid line) of the differential conductance curve (open circles) at  $T = 7.7$  K with the one-gap model.

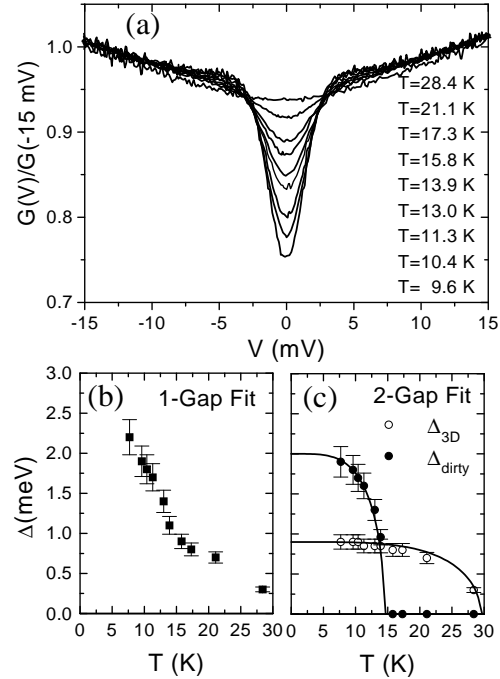


FIG. 4. (a) Normalized differential conductance curves for increasing (bottom to top) temperatures. (b) Temperature dependence of the order parameter from fit with the one-gap model. (c)  $\Delta_{dirty}(T)$  and  $\Delta_{3D}(T)$  from fit with the two-gap model. Fit to BCS curves (solid lines) is also shown .